5493-1

APPENDIX B

Effects of Aircraft Wake Dynamics on Measured and Simulated NO_x and HO_x Wake Chemistry

D.C. Lewellen and W. S. Lewellen

Journal of Geophysical Research
Vol. 106, No. D21, pages 27,661-27,672
16 November 2001

Effects of aircraft wake dynamics on measured and simulated NO_x and HO_x wake chemistry

D. C. Lewellen and W. S. Lewellen

Department of Mechanical and Aerospace Engineering, West Virginia University, Morgantown, West Virginia, USA

Abstract. High-resolution numerical large-eddy simulations of the near wake of a B757 including simplified NO_x and HO_x chemistry were performed to explore the effects of dynamics on chemistry in wakes of ages from a few seconds to several minutes. Dilution plays an important basic role in the NO_x – O_3 chemistry in the wake, while a more interesting interaction between the chemistry and dynamics occurs for the HO_x species. These simulation results are compared with published measurements of OH and HO_2 within a B757 wake under cruise conditions in the upper troposphere taken during the Subsonic Aircraft Contrail and Cloud Effects Special Study (SUCCESS) mission in May 1996. The simulation provides a much finer grained representation of the chemistry and dynamics of the early wake than is possible from the 1 s data samples taken in situ. The comparison suggests that the previously reported discrepancy of up to a factor of 20 - 50 between the SUCCESS measurements of the $[HO_2]/[OH]$ ratio and that predicted by simplified theoretical computations is due to the combined effects of large mixing rates around the wake plume edges and averaging over volumes containing large species fluctuations. The results demonstrate the feasibility of using three-dimensional unsteady large-eddy simulations with coupled chemistry to study such phenomena.

1. Introduction

The possibility that future increases in the commercial aircraft fleet may have significant environmental and climatological effects is being widely studied [e.g., *Penner et al.*, 1999; *Schumann*, 1998; *Friedl*, 1997]. While the volume of aircraft emissions is not large compared to ground-based sources, these emissions are injected directly into the relatively stable upper troposphere and lower stratosphere where small emissions may have potentially significant effects. A number of field programs have been conducted, e.g., Subsonic Aircraft Contrail and Cloud Effects Special Study (SUCCESS) [*Toon and Miake-Lye*, 1998], SASS Ozone and Nitrogen Oxide Experiment (SONEX) [*Singh et al.*, 1999], and AERONOX [*Schumann*, 1997], which use in situ measurements in wakes as a means to better determine the aircraft emissions and understand the chemical kinetics within the wake plume. Our subject in this work, the effects of wake dynamics on wake chemistry measurements, is an important source of uncertainty in interpreting the results of such field measurements or results from atmospheric chemistry models. When the sampling volumes being measured (or modeled) contain large fluctuations of some chemical species, the average concentration measured and chemistry inferred may be quite different from the local results occurring within that volume. This is particularly true when reaction rates between relevant species are faster than turbulent mixing rates, allowing strong anticorrelated distributions to occur. This necessarily reduces the effective reaction rate of average concentrations, making those rates dependent on mixing rates in the fluid [*Sykes et al.*, 1992; *Schumann*, 1989].

Here our focus is on the dynamics and chemistry within a wake plume from an age of a few seconds to several minutes. This is a regime which has been heavily studied in in situ measurement campaigns. It includes the partial capturing of the exhausts by the trailing

vortex pair behind the aircraft, the vortex-dominated dynamics which dramatically expand the wake plume both vertically and horizontally, and the subsequent buoyant oscillations of the plume after the vortex dynamics subside. We do not consider the chemistry in the earliest jet exhaust phase where temperatures are initially very high but rapidly dilute toward ambient levels, or the ultimate fate of the wake plume and its chemical constituents at late times where the dynamics are dominated by ambient atmospheric turbulence, although both are likely to prove important in assessing the environmental effects of aviation.

During this time period we are particularly interested in the impact of species fluctuations on scales that are typically too small to be measured by trailing aircraft moving at speeds often in excess of 200 m s^{-1}. Accordingly, we utilize a three-dimensional (3-D), unsteady, high-resolution model of the aircraft wake which is capable of resolving dynamical and/or chemical features on scales of a few meters. The large-eddy simulation (LES) code we employ for the fluid dynamics is the same one used by *Lewellen and Lewellen* [1996] to present detailed dynamics of the vortex pair breakup in an aircraft wake; by *Lewellen et al.* [1998] to compare numerical simulation results of wake dispersion to lidar observations; and by *Lewellen and Lewellen* [2001] to examine effects of wake dynamics on contrail evolution. Given the computational requirements of the resolution we employ, we can include only a limited set of chemical reactions and species within our simulations. Nonetheless, this proves sufficient to demonstrate some potentially important effects, while confirming the practical feasibility of coupling detailed dynamics and chemistry using LES.

Of particular interest to us in this study were a set of HO_x measurements taken during SUCCESS [*Tan et al.*, 1998]. These showed an apparently anomalously high ratio of $[HO_2]/[OH]$ within young wake plumes, 20 – 50 times greater than expected by simple chemical computations. The authors suggested that this effect might be due in part to the strong anticorrelation between NO and HO_2 in the turbulent fluctuations within the wake occurring during these measurements. To quantitatively test this possibility, we have included HO_x chemistry in addition to basic NO_x – ozone chemistry in our reaction set for the present work, and have chosen to simulate a B757 wake with nominal conditions and emissions in agreement with those reported during the SUCCESS HO_x measurements.

Our approach here is complementary to other recent studies of chemistry in aircraft wake plumes. These include studies of detailed chemistry in the early hot jet regime coupled with simple dynamics [e.g., *Miake-Lye et al.*, 1993; *Menon and Wu*, 1998; *Kärcher et al.*, 1998]; studies with detailed chemistry in the wake vortex regime with dynamics modeled in two dimensions [e.g., *Anderson et al.*, 1996]; studies of older plumes with detailed box model chemistry but only rudimentary dynamics included via some prescribed dilution history [e.g., *Karol et al.*, 1997]; studies with detailed 3-D aircraft wake dynamics but only passive tracers for the engine exhausts [e.g., *Lewellen and Lewellen*, 1996; *Gerz and Ehret*, 1996; *Gerz et al.*, 1998; *Lewellen et al.*, 1998]; and studies of ice phase "chemistry" (contrails) interacting with wake dynamics at many different levels of approximation [e.g., *Gierens*, 1996; *Chlond*, 1998; *Sussmann and Gierens*, 1999; *Gierens and Jensen*, 1999; *Lewellen and Lewellen*, 2001; *Sussmann and Gierens*, 2001]. Aircraft wake dynamics alone, ignoring the fate of the engine exhaust products, have also been a significant area for research because of potential effects on closely following aircraft and the resulting safety issues for takeoff and landing at airports. A recent review of these efforts, including some large eddy and direct numerical simulations, has been made by *Spalart* [1998].

In section 2 we provide an overview of our LES model and the conditions simulated. In section 3, we discuss the simulation results, beginning with the basic wake dynamics and NO_x – ozone chemistry, as illustrated by the simulations, and ending with the dramatic effects of dynamics on measured HO_x chemistry in the wake. A summary and some final comments follow in section 4.

2. Model Overview and Simulation Conditions

In order to simulate detailed wake dynamics, species dispersion, and the accompanying chemistry, we use the technique of numerical large-eddy simulation. The range of length scales involved in this problem is much too great to permit a direct numerical simulation of all scales with currently available computer resources. Instead, we solve the Navier–Stokes equations directly for the most important scales in the flow (from smaller than the wake vortex core size to many times the aircraft wingspan), but only model the effects of the smaller, unresolved eddies. Our simulation is of a B757 flying in the upper troposphere under cruise conditions, nominally that relevant for the SUCCESS observations. Details of our LES model applied to aircraft wake dynamics have been given by *Lewellen and Lewellen* [1996, 2001], along with a discussion of the many choices and com-

promises necessarily involved in efficiently tackling such simulations. A summary of the model and simulation conditions is given below, first for the fluid dynamics and then for the chemistry added specifically for the present work.

2.1. Fluid Mechanics

The LES code we employ for aircraft wake simulations is a modified version of one we use for boundary layer cloud modeling [e.g., *Lewellen and Lewellen*, 1996], which in turn is based on the implementation of *Sykes and Henn* [1989]. It is a 3-D finite difference implementation of the incompressible Navier-Stokes equations in the Boussinesq approximation, second-order accurate in space and time. It incorporates a piecewise parabolic model algorithm for the advection of thermal energy and species concentrations. The pressure field is obtained by directly solving the Poisson equation using fast Fourier transforms in the downstream direction, the method of *Farnell* [1980] for nonuniform grids in the cross-stream direction, and a tridiagonal solver in the vertical.

The simulation of the interacting trailing vortex pair in an aircraft wake presents a particular challenge because both small grid spacings and large domains are required. A grid spacing of a few percent of the wingspan or less is required to resolve the trailing vortex cores and the transport of the engine exhausts around and into them. At the same time, line vortices have a sizable long-range influence on the flow field, so domain widths of several wingspans or more are required to minimize unwanted boundary interactions. We employ three devices to help to meet these conflicting demands: (1) a stretched grid spacing in the vertical and cross-stream directions to achieve fine spacing where it is needed within the wake while maintaining large domain sizes; (2) vertical tracking of the wake to insure that the fine grid portion of the domain encompasses the descending wake vortices; and (3) different grids (six in the case presented here) for different segments of the simulations as the wake evolves and the optimum grid requirements change. A variable time step was used in the simulation, with values ranging from 0.003 to 0.02 to 1 s for, respectively, the early jet, early vortex, and late time stages discussed below.

We employ a subgrid model which uses a quasi-equilibrium, second-order turbulence closure scheme with the subgrid turbulent kinetic energy carried as a dynamical variable and the maximum subgrid turbulence length scale related to the numerical grid length. The damping of subgrid turbulence by a stable temperature gradient or a stable rotational velocity field is approximately included via appropriate reductions of the subgrid turbulence length scale. The incorporation of rotational damping effects in the subgrid model is somewhat unusual, but useful for simulations of strong vortices in order to avoid unphysically large rates of core diffusion. The method is described in detail by *Lewellen et al.* [2000], who used it extensively in tornado simulations. It was not included in our earliest aircraft wake simulations [*Lewellen and Lewellen*, 1996], but has been used since [*Lewellen et al.*, 1998; *Lewellen and Lewellen*, 2001].

We employ periodic boundary conditions in all three directions. Effectively, this means there are neighboring wakes located at twice the distance to the boundary in the vertical and crosswise directions evolving in parallel with our simulated wake. The stretched grid allows us to place the boundaries at sufficient distance to make the effects of these image vortices negligible. Periodicity in the vertical is modified by a temperature shift between the top and bottom of the domain to permit a mean stratification to be imposed. In imposing periodic conditions in the downstream direction we are treating the wake portion within our domain as if it were laid down instantaneously. This is an appropriate approximation here because the aircraft flight speed is much greater than the velocity scales of the wake dynamics over the period treated (which excludes the region within a few wingspans of the aircraft). The approximate periodicity of the wake downstream is amply confirmed by observations of contrail evolution from ages of a few seconds to several minutes.

The initial conditions were chosen consistent with cruise conditions for a B757 flying at 11 km altitude at 210 m s^{-1}, with a mass of 87,000 kg (which is midway between the minimum and maximum masses for this aircraft). For an effective vortex pair separation of 29.4 m this implies a circulation about the vortices of 380 m^2 s^{-1}. The heat produced by the engines per meter of flight path was taken as 255 K m^2, computed from a total fuel flow rate of 3.1 kg km^{-1} (in agreement with that quoted for the SUCCESS measurements by *Tan et al.* [1998]), a specific combustion heat of 43 MJ kg^{-1} appropriate for kerosene-type jet fuels, and an assumed jet engine efficiency of 30%. The integrated momentum in the exhaust jets per meter of flight path was chosen as 502 m^3 s^{-1}, computed from the assumed fuel flow rate, flight speed, and a specific fuel consumption of 16.9 mg N^{-1} s^{-1}. The detailed cross-stream distributions of the velocity fields and exhaust products depend on the roll up of the vorticity shed from the wing and

were taken from a UNIWAKE simulation [*Quackenbush et al.*, 1996], with values scaled so as to match the desired circulation, jet momentum, engine heat, etc.

As we will discuss in detail below, the fluctuations in exhaust distribution play an important role in affecting measured chemistry in the wake. Accordingly, we have at least approximately included the effects of exhaust jet turbulence into the initial conditions used for our chemistry simulation. This was done by performing an initial simulation of the early wake (without chemistry) from an age of about 0.5 s to 3.5 s, with high spatial resolution (0.33 m finest grid spacing), for a short (42 m) downstream portion of wake, to develop some jet turbulence and smaller-scale fluctuations in the exhaust distribution. These results were periodically continued to provide the initial conditions for the full downstream domain employed for the chemistry simulation.

To complete the initial conditions for our simulations, the aircraft wake is superimposed with an ambient atmospheric field (the result of a separate large-eddy simulation), as described by *Lewellen and Lewellen* [1996]. The field was generated in the desired domain, with a nominal value of potential temperature stratification for the upper troposphere (2.5 K km^{-1}) and no mean wind shear. Large initial velocity and temperature perturbations were applied and the subsequent evolution followed via LES until the turbulence and gravity waves had a chance to adjust to the stratification, and their amplitude had decayed into a reasonable range (turbulent dissipation rate of order 2×10^{-5} $m^2 s^{-3}$).

Table 1 summarizes the grids employed for the primary simulation. The choice of grid for the given segment of the simulation was correlated with the wake vortex dynamics then occurring, in order to best apportion the limited number of grid points available given the physics that had to be resolved. As the dynamics progress the wake expands and turbulence levels fall, so that the finest grid spacing can be increased on subsequent grids but must cover larger portions of the domain. Accordingly, when the wake dynamics would threaten to outgrow the fine-grid region of the domain, we simply interpolated the species and flow fields to a more suitable grid. The domain size was doubled for the fourth grid. To do this, the final field generated on the third grid was periodically doubled in the downstream direction and added to an ambient turbulence field generated by a separate LES on the doubled domain.

As noted previously, the vertical and cross-stream domain edges were chosen far from the wake to minimize boundary effects and allow a more realistic ambient turbulence field. There is a different constraint on the downstream domain size as discussed at length by *Lewellen and Lewellen* [1996]. The downstream domain size must be commensurate with the period of the basic wake decay mode, the Crow instability (discussed below). For a given aircraft, there is considerable variability in the observed periodicity, depending on the wave and turbulence spectrum in the ambient atmosphere. It is not unusual to see a factor of 2 variation in period within a single contrail in the sky. Nonetheless, there is a preferred range of wavelengths encountered. Here we choose a downstream domain dimension of 210 m, expecting a Crow period of approximately that length, which for the B757 is a little less than the wavelength of maximum amplification deduced by *Crow* [1970] from a linear stability analysis, and a little greater than the most favored range found in the direct numerical simulation study of *Spalart and Wray* [1996]. In previous work we have found little variation of the basic wake decay (rate of wake dispersion, overall vertical and horizontal extent, wake lifetime, etc.) with downstream domain size. The interaction between a given Crow period and its neighbors is only weakly affected by the detailed structure of those neighbors, so replacing them with periodic images proves to be a reasonable approximation. Providing for multiple Crow periods to be simulated does give additional turbulent realizations of these structures. We performed an additional simulation analogous to the one presented here but with a different ambient turbulence field (with lower turbulence intensity) to estimate the variation in our chemistry results between different turbulent realizations of the same basic process. For the summary results presented below, the two sets of results were all very close.

2.2. Chemistry

Given the number of grid points in our simulations, we use a relatively simple (and therefore numerically less costly) chemical reaction set, concentrating on important reactions within the wake plume for ages from a few seconds to a few minutes. The chemical species considered are NO, NO_2, HONO, HNO_3, O_3, OH, HO_2, CO, and CH_4, with basic reactions:

$$NO + O_3 \longrightarrow NO_2 + O_2, \quad (1)$$

$$NO_2 + h_\nu + O_2 \longrightarrow NO + O_3, \quad (2)$$

$$HONO + h_\nu \longrightarrow OH + NO, \quad (3)$$

$$OH + NO \longrightarrow HONO, \quad (4)$$

$$OH + NO_2 \longrightarrow HNO_3, \quad (5)$$

Table 1. Grids Used for the B757 Chemistry Simulation[a]

Grid	Domain, m	Number of Grid Points	Fine Spacing, m	Time period, s
0	660x660x42	162x154x130	0.33x0.33x0.33	0.5–3.5
1	660x800x210	124x116x130	0.8x0.8x1.6	3.5–50.
2	660x800x210	120x121x162	1.x1.x1.3	50–100
3	660x900x210	152x134x130	1.6x1.6x1.6	100–240
4	1200x1300x420	100x139x122	3.3x3.3x3.5	240–500
5	1200x1300x420	94x119x66	6.5x6.5x6.5	500–900

[a]Domain dimensions, number of grid points, and fine grid spacings are given for the (cross-stream)x (vertical)x(downstream) directions, respectively. Grid 0 was used for an initial simulation without chemistry to generate initial conditions including turbulent jet fluctuations for the main simulation.

$$HO_2 + NO \longrightarrow OH + NO_2, \quad (6)$$

$$OH + CO + O_2 \longrightarrow CO_2 + HO_2, \quad (7)$$

$$OH + O_3 \longrightarrow HO_2 + O_2, \quad (8)$$

$$HO_2 + O_3 \longrightarrow OH + 2O_2, \quad (9)$$

$$OH + CH_4 + ... \longrightarrow HO_2 + NO_2 + ... \quad (10)$$

The reaction rates employed ($k_{NO+O_3} = 2.39\times10^{-5}$, $k_{OH+NO} = 4.63\times10^{-2}$, $k_{OH+NO_2} = 9.18\times10^{-2}$, $k_{HO_2+NO} = 8.4\times10^{-2}$, $k_{OH+CO} = 1.29\times10^{-3}$, $k_{OH+O_3} = 1.59\times10^{-4}$, $k_{HO_2+O_3} = 8.32\times10^{-6}$, $k_{OH+CH_4} = 5.2\times10^{-6}$, all in (ppb s)$^{-1}$) were taken from *DeMore et al.* [1997] for conditions of 217 K and 0.224 atm, except for the OH + NO_2 reaction rate, which was taken from *Brown et al.* [1999]. Nominal daytime values at 11 km altitude were chosen for the photolysis rates ($J_{NO_2} = 0.01$ s^{-1} and $J_{HONO} = 0.0033$ s^{-1}). Reaction (10) is an effective one for the cycling of OH to HO_2 through the intermediary CH_3O_2 in the presence of NO. It is only of minor importance to the HO_x chemistry in the regime being studied (being dominated by reaction (7)), but is included approximately at little extra numerical cost by taking the CH_4 concentration as constant. The variations of the rate constants due to temperature fluctuations within the wake plume have not been included here. For the wake ages considered, the variations in temperature encountered are generally of order a degree or less, giving changes in rate constants of a few percent or less (which is generally below the level of uncertainty in the rate formulas themselves).

In choosing the initial chemical concentrations, we did not try to match a particular SUCCESS flight condition, but did pick values within the ranges measured during the SUCCESS flights: ambient background levels of HO_2 between 10-20 pptv and OH between 0.3-0.5 pptv [*Tan et al.*, 1998]; ambient levels of NO_x = 70 pptv, CO = 120 ppbv, O_3 = 65 ppbv, and CH_4 = 1750 ppbv [*Jaegle et al.*, 1998]. The actual values used for the HONO, OH, and HO_2 concentrations (HONO = 0.36 pptv, OH = 0.42 pptv, and HO_2 = 15 pptv) and the split of NO_x into NO and NO_2 (NO = 55 pptv and NO_2 = 15 pptv), were also chosen so that the background concentrations of any species did not drift significantly over the course of the simulation (realizing that other reactions besides those explicitly treated are important in setting the background equilibrium concentration over timescales much longer than we consider here).

The initial concentration used for each species consisted of a background level plus a plume concentration, with the latter chosen consistent with measured emission indices, fuel consumption rates, and flight speeds for the SUCCESS flights. In particular, the NO emission index is taken as 7.5 g NO_2 kg^{-1} fuel [*Campos et al.*, 1998], with a total fuel usage per flight path of 3.1 g m^{-1}. The volume ratio of CO above background in the exhaust to NO_x was set at 0.306, consistent with the median emission index (1.55 g kg $^{-1}$) measured on May 4 during SUCCESS [*Vay et al.*, 1998]. The ratios of HONO and NO_2 to NO_x in the jet are set at nominal values of 0.04 and 0.1, respectively. The initial plume excesses over background for HNO_3, O_3, CH_4, OH, and HO_2 were taken to be zero.

The biggest numerical costs of including chemical reactions within our LES are the added memory required for the 3-D species fields and the added computation

involved in advecting and diffusing them as governed by the flow field. Accordingly, it is useful to minimize the number of species which must be carried as dynamical variables. We reduce this number by two by identifying three combinations which are conserved by equations (1)–(10) (so that their plume concentrations above background always remain proportional to each other): NO + NO_2 - OH - HO_2 (essentially NO_x within the plume); HO_2 + OH + HONO + HNO_3 (which we use after the computation to solve for HNO_3); and CO (which is conserved to a high degree of accuracy because the CO levels everywhere are so much greater than the OH levels which erode it via (7)).

In numerically implementing (1)–(10), one point requires particular care. Some of the reactions involving OH and HO_2 (equations (4)–(6)) proceed on a very short timescale within the core of the wake plume where the NO_x concentrations are high, shorter than the time step required to accurately follow the flow dynamics. We cannot simply use equilibrium values for OH and HO_2 because the timescale for the relevant reactions does not remain small (compared to the time step appropriate for the flow dynamics) within the edges of the plume. Instead, we update the OH and HO_2 chemistry semi-implicitly. In short domain tests we have confirmed that the simulated OH and HO_2 concentrations evolve correctly in time within the plume edges, while giving the correct equilibrium values within the plume core, regardless of the time step chosen. The remaining reactions progress on timescales which are comparable to or slower than the flow timescales; consequently, the chemistry for the species other than OH and HO_2 are updated explicitly in time.

3. Results

The chief impact of wake dynamics on the chemistry is through plume mixing. This reduces concentrations of exhaust constituents, mixes fresh ambient air with plume air, and produces fluctuations in plume distributions. It is appropriate, then, in explaining the simulation results, that we begin with a summary of a typical wake decay history and its effects on passive plume dispersal. Simple NO_x – O_3 chemistry is considered next before turning to HO_x chemistry, where we find the most interesting effects of dynamics on chemistry illustrated by our simulations.

3.1. Review of Basic Wake Decay Mode and Species Dispersion

Figure 1 illustrates some of the simulated wake dynamics out to an age of 10 min, as visualized by the cross-stream integrated NO_x distribution in the wake plume. Since NO_x is essentially a conserved species, the distribution shown is a result of dispersion only. The format is as described by *Lewellen et al.* [1998], inspired by scanning lidar measurements of wakes. The wake is sampled as if it were being advected at a steady rate by a mean wind aligned with the wake. The horizontal axis then varies over time and downstream distance so that both the temporal evolution and spatial structure can be seen. The "drift velocity" determining the unit of distance per unit of time has been chosen to be 9.5 m s^{-1}, which is in a convenient range for displaying both the temporal and spatial structure. In the figure the vertical distance scale has been expanded by a factor of 3 relative to the downstream distance scale for clarity.

The main features of the wake evolution can be followed in this figure. We give only a brief summary of the dynamics here; more detail may be found in our previous papers. The early wake dynamics are dominated by the vortex pair which results from the lift generated by the aircraft's wings. For the first minute or so the vortex pair descends rapidly. Initially, the engine exhaust distribution is stretched and advected by the velocity field accompanying the vortex pair, giving a period of very rapid dilution. Subsequently, the exhausts are partitioned into three different populations: relatively high concentrations in and immediately around the vortex cores where mixing rates are low; midlevel concentrations and mixing rates within the ellipse of fluid surrounding and descending with the vortex pair; and lower concentrations and higher mixing rates within a fraction of the exhausts which is not ultimately entrained into the falling vortex system (or becomes detrained from it) and remains close to flight level. The fraction of exhausts finding its way into each population is most strongly influenced by the engine placement of the particular aircraft, but is also influenced to a lesser extent by the atmospheric turbulence levels, shear, and stratification.

While the vortices descend, perturbations of the vortices from the ambient atmosphere (and/or unsteady wing loading or jet turbulence) grow via the Crow instability [*Crow*, 1970] . The rate of growth depends primarily on the wavelength of the perturbation, the vortex spacing, and circulation. In a turbulent atmosphere the vortices see a superposition of perturbations, and the instabilities for different wavelengths compete

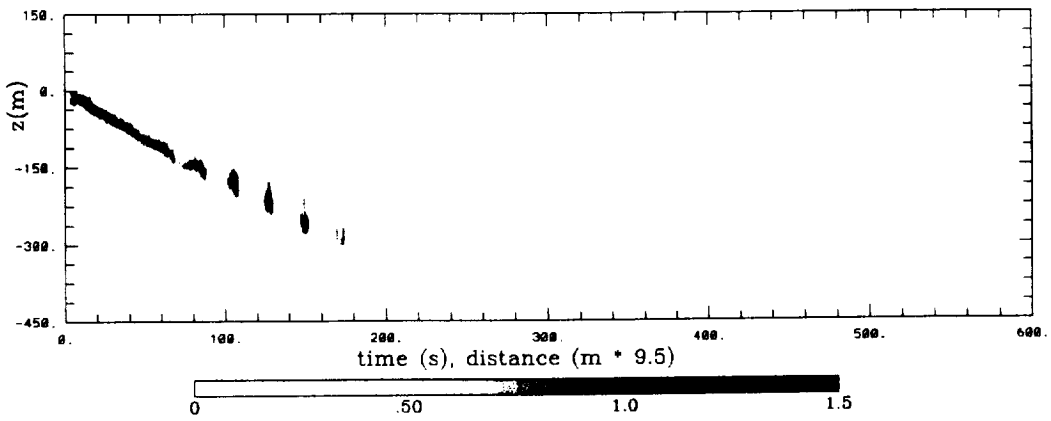

Figure 1. Downstream space/time versus height plot of cross–stream integrated plume NO_x (in ppm m) for a simulated B757 wake.

with each other. Those which are in the range of most rapid growth and have the largest initial perturbations eventually win out.

The growth of the Crow instability proceeds until the vortices touch, reconnect, and form elongated vortex rings. This occurs at a wake age of around 80 s in the present B757 simulation. During the reconnection process some of the exhausts escape from the vortex system and buoyantly rise. The distribution of the remainder is significantly scrambled so that the peak concentrations no longer provide a clear signature of the vortex dynamics. The vortex rings continue to descend and, at the same time, open up in the cross-stream direction, thereby significantly increasing both the vertical and horizontal extents of the wake. They can further interact with themselves, even sometimes relinking again to form two rings from one. This, together with the continual diffusion of the vortex cores (due to the smaller-scale atmospheric turbulence and interaction with the ambient stratification), eventually leads to the demise of the organized vortex system. In the present simulation the descent of the vortex rings (or their remnants) continues until an age of approximately 230 s, with about half of the total wake descent (of ~320 m) occurring after the pair initially relinks. It is the descending vortex rings which (for appropriate ambient humidity) give rise to the periodic series of puffs often seen in contrails.

The coherent wake dynamics do not end with the dissolution of the wake vortices. The positive buoyancy acquired by the vortex system's descent through the stratified atmosphere (together with the heat in the initial engine exhaust) drives a strong Brunt-Väisälä oscillation. In the absence of significant wind shear, we find that this oscillation drives the dominant turbulence that mixes the wake plume until it damps, after 1-3 Brunt-Väisälä periods, to the level of the ambient atmospheric turbulence. The Brunt-Väisälä oscillation can be seen in the long-timescale (10 min period) vertical modulation evident in Figure 1.

There are variations in the details of this basic wake decay mode depending on aircraft and atmospheric conditions, but that illustrated is typical. We have found in simulations of wakes and observations of contrails that the dynamics of the Crow instability primarily govern the wake decay for a wide range of conditions in the absence of large wind shear.

3.2. NO_x - Ozone Chemistry

Figures 2-4 summarize the evolution of several chemical species during the wake decay. All of the concentrations plotted are excesses above (or below) the constant background level. Consider first the evolution of the NO, NO_2, and HONO concentrations. These are dominated by plume dispersion. The local peak concentrations of these species fall sharply (Figure 2) for the first ~25 s as the jet exhausts mix throughout the ellipse of fluid falling with the vortex pair. Subsequently, they fall nearly linearly while the vortex-driven turbulence dominates and more slowly when the vortex system dissolves and the weaker Brunt-Väisälä sloshings take over. There is a noticeable enhancement in the dilution rate of the peak concentrations for a period after vortex linking occurs, with its accompanying scrambling of the exhausts. The peak local concentrations are located within the lowest (vortex-dominated) part of the wake plume until about the 250 s point, after which the

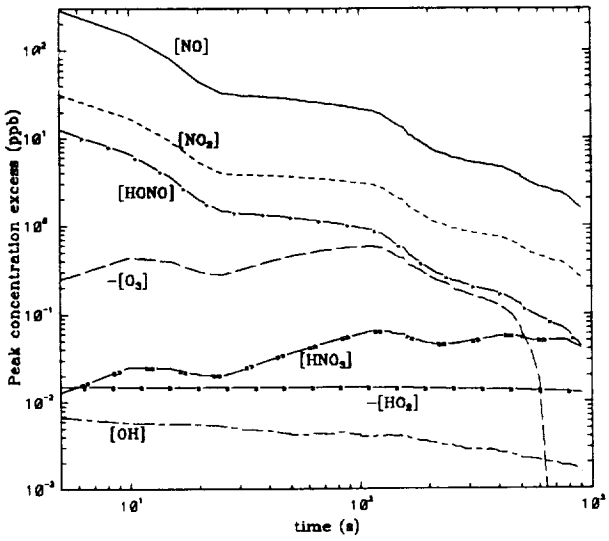

Figure 2. Peak concentrations of chemical species in the wake relative to background versus time.

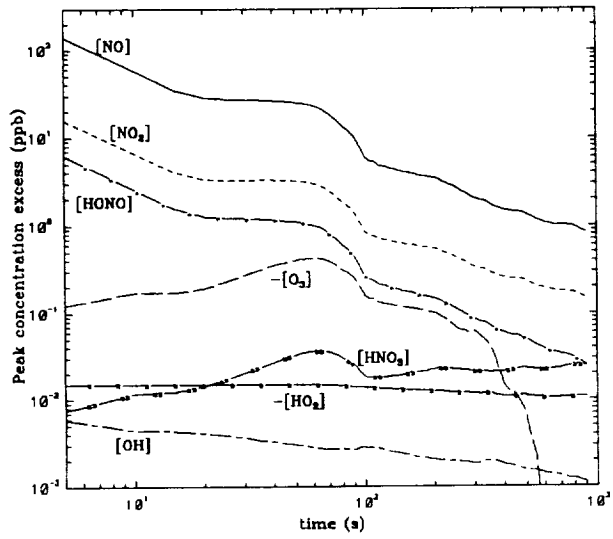

Figure 3. Peak downstream averaged wake plume concentrations relative to background versus time.

peak is located near the original flight level, within the upper wake (which, being less turbulent, dilutes at a slower rate).

In an in situ measurement, a following aircraft obtains not a strictly local concentration, but the average over some finite sampling volume. A corresponding plot of peak measured concentration versus plume age would

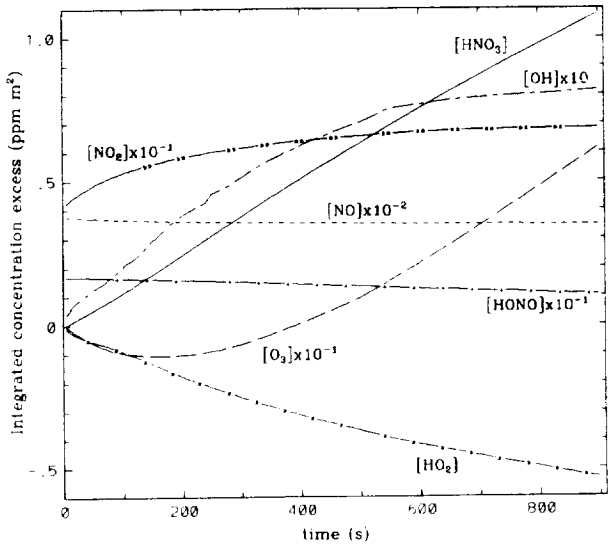

Figure 4. Integrated wake plume concentrations above background per meter of flight path versus time.

look more like that in Figure 3 (corresponding to 1 s samples of a chase aircraft maintaining a constant separation behind the lead aircraft). The NO, NO_2, and HONO concentration histories in Figure 3 are well correlated with those in Figure 2, but with some noticeable differences. The downstream average peak concentrations drop much more steeply between about 50 and 100 s as the vortices are twisted by the growing Crow instability. The peak measured concentrations remain located with the vortices during this period, but subsequently shift to the exhausts released by the vortex system during the linking process. These buoyantly rise to rejoin the upper wake at about 180 s.

The plume-integrated amounts of NO, NO_2, and HONO vary much more slowly, in response to the wake chemistry itself (Figure 4). The plume NO is slowly converted to NO_2 via (1); the initial ratio of $[NO_2]/[NO]$ = 0.11 will eventually rise to approach its background equilibrium value for the present conditions of 0.27 as the plume dilutes. The total HONO is slowly depleted via photolysis, with a corresponding nearly linear rise in HNO_3 to approximately 2.6% of the plume NO_x at 900 s. The time evolution of the peak HNO_3 concentration (Figure 2) represents a competition between this production and the plume dilution.

The OH and HO_2 behavior in the plume are qualitatively different. As we will discuss in more detail below, the differences from background for these species are more nearly constant within the plume, so that the

integrated contribution scales approximately with the plume volume. There is a sharp initial increase associated with the early mixing of the exhaust jets by the vortices, a nearly linear increase for the next 200 s as the descending vortices and oscillating vortex rings stretch the plume volume both vertically and horizontally, and a slower rate of increase as the vortices dissolve and the Brunt-Väisälä oscillations take over and slowly subside (Figure 4).

The O_3 evolution is more interesting, and we might expect more subtle interplay between the chemistry and dynamics for this species since both the NO photolysis and NO + O_3 reaction (for early plume NO concentrations) occur with characteristic timescales of order 100 s, a timescale which is also of importance for the wake dynamics as seen in Figure 1. The destruction of O_3 by NO within the plume is larger than the production via NO photolysis for the first ~170 s (Figure 4) and reversed afterward so that an O_3 deficit forms but is later replaced by an O_3 surplus, with the age of the crossover point strongly influenced by the plume dynamics. The magnitudes above or below background are all small, however. At the given NO concentrations, equation (1) has difficulty competing with the level of plume dilution continually mixing in fresh O_3 from the air outside the plume. If either the NO concentration had been an order of magnitude larger, or the plume dilution rates that much smaller, the chemistry and dilution rates would have been comparable and the interaction between the two would have been more complex. An even larger change would make the chemistry fast compared to the mixing, and a much stronger anticorrelation between NO and O_3 would have developed(as seen in the works by *Schumann* [1989] and *Sykes et al.* [1992]).

3.3. HO_x Chemistry

The effects of the three-dimensional wake dynamics are much more dramatic for the OH and HO_2 chemistry, and can explain a puzzle found in the in situ observations of *Tan et al.* [1998]. In a series of observations during SUCCESS. OH, HO_2, and NO concentrations were measured within the wake plume of a B757 for wake ages from about 10 to 100 s. The measuring DC-8 also sampled its own wake at much later ages (about 1200 s). As expected (and as we find here), the measured OH levels sharply rose upon entering the plume, while the HO_2 levels sharply fell (cf. their Figure 1).

The measured ratio of HO_2/OH concentrations as a function of NO, however, was about 20–50 times larger than expected (cf. their Figure 2). As the authors argued, within the plume where the NO levels are high the sources and sinks of OH and HO_2 are slow compared to the exchange reactions between them, so that the ratio is, to good approximation,

$$\frac{[HO_2]}{[OH]} = \frac{k_{OH+CO}[CO]+k_{OH+CH_4}[CH_4]+k_{OH+O_3}[O_3]}{k_{HO_2+NO}[NO] + k_{HO_2+O_3}[O_3]}. \quad (11)$$

It is this prediction which is sometimes greatly exceeded by the observations.

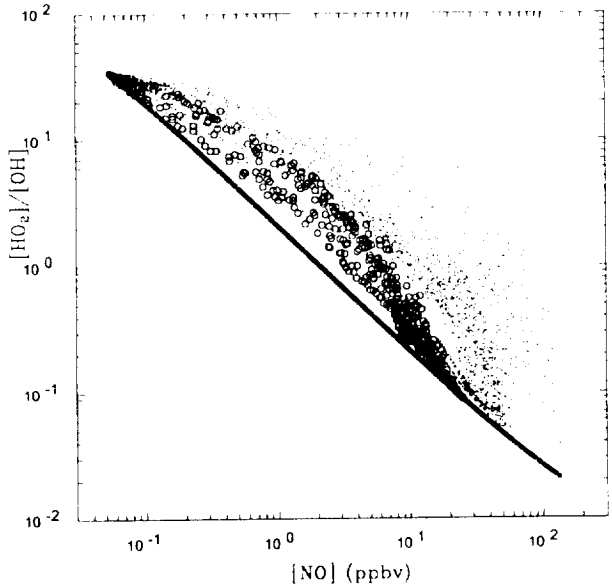

Figure 5. Apparent $[HO_2]/[OH]$ ratio deduced from simulation data using 210 m sample lengths, versus the equilibrium expectation (thick line). Small points are sampled from wake plumes of ages 6 and 10 s; open circles for plume at 50 s.

Figures 5 and 6 show our simulated $[HO_2]/[OH]$ ratio for sample measurements. The format is as in Figure 2 of *Tan et al.* [1998] (except for the log scale and sorting the data by wake plume age), with the data sampled in analogous fashion. The time resolution for the measurements was 1 s, which at the average flight speed of 210 m s^{-1} of the measuring aircraft means an average over 210 m for each data sample. Accordingly, the simulated measurements in Figures 5 and 6 are 210 m averages sampled along lines parallel with the flight track at many positions within the simulated wake, at ages as noted. As in the observations, the analogous $[HO_2]/[OH]$ measurement from the simulation shows values ranging up to 50 times greater than the local equilibrium predictions (thick line).

In our simulated chemistry there are two main effects

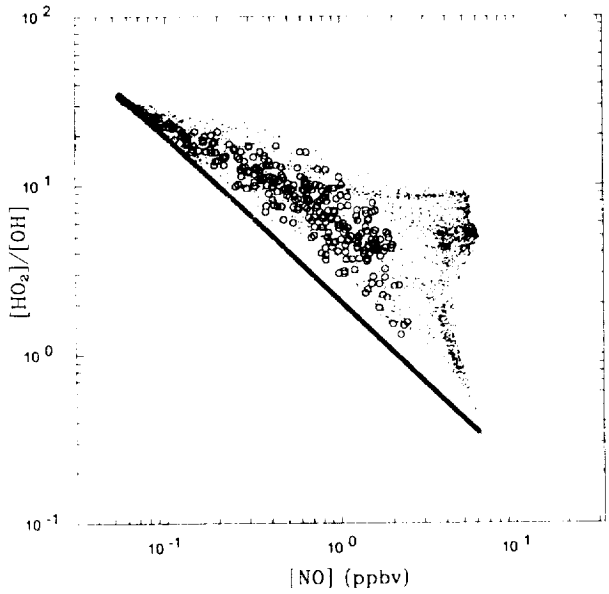

Figure 6. As in Figure 5, but for wake plume ages of 100 s (dots), and 250 s (circles).

responsible for this discrepancy, both of which critically involve the wake dynamics. The first stems from the difficulty with using spatially averaged samples in (11) when there are significant species fluctuations within the sampling volume. The second arises because the equilibrium assumption in (11) is no longer valid around the edges of the plume. Let us consider each of these effects, in turn, in more detail.

Figure 7 shows the evolution of the simulated OH and HO_2 concentrations on a vertical streamwise slice through the wake. The format is as in Figure 1 except the fields are not cross-stream integrated but lie on a single plane parallel to the wake, initially situated midway between the aircraft centerline and one of the trailing vortices. The vertical and downstream lengths are plotted at the same scale in this figure. In most of the plume volume at any given time OH is nearly constant, HO_2 is very small, and (though it is not readily apparent from the figure) equation (11) is well satisfied. However, it is clear that our 210 m downstream samples will in general include a wide range of plume conditions, sometimes both high plume concentrations and air outside of the plume. This sampling effect influences the measured HO_2 in the plume more than the measured OH, and the ratio still more because OH and HO_2 are strongly anticorrelated. This can be seen as follows. Within the plume, where NO is large and the OH-HO_2 exchange reactions are fast, the dominant source of OH and HO_2 is HONO photolysis, and their concentrations are well represented by the equilibrium values:

$$[\mathrm{OH}] = \frac{J_{\mathrm{HONO}}[\mathrm{HONO}]}{k_{\mathrm{OH+NO}}[\mathrm{NO}] + k_{\mathrm{OH+NO_2}}[\mathrm{NO_2}]}, \quad (12)$$

$$[\mathrm{HO_2}] \approx [\mathrm{OH}]\frac{k_{\mathrm{OH+CO}}[\mathrm{CO}]}{k_{\mathrm{HO_2+NO}}[\mathrm{NO}]}, \quad (13)$$

where the last equation follows from keeping the dominant terms in (11). The HONO, NO, and NO_2 concentrations vary strongly within the plume, but this is due mostly to dilution, which acts on each of these species in essentially the same way. The ratios of these species (along with OH via (12)) then vary little within the plume and relatively slowly in time. In contrast, HO_2 in the plume varies approximately as [OH]/[NO] since CO is approximately constant (there is a plume contribution to CO but it is generally well below the background contribution except for the peak values at the earliest times in our simulation, when they are comparable). In the plume, then, we have approximately $[HO_2]/[OH] \sim 1/[NO]$ (which is why the prediction from (11) gives a nearly linear curve on the log-log plots of Figures 5 and 6). The averaging from the finite sample size affects the measurements on the two axes in Figures 5 and 6 very differently. The correlation of the averages $\langle 1/[NO] \rangle$ and $\langle [NO] \rangle$ differs greatly from the correlation of point samples of 1/[NO] and [NO] because of the nonlinearity of the function being averaged. When averaging over sample volumes containing large fluctuations of the NO field, $1/\langle [NO] \rangle$ and $\langle 1/[NO] \rangle$ are clearly significantly different functions, the latter being disproportionally enhanced relative to the former by the contribution of regions with low NO. Moreover, if some air outside of the plume (where (12) and (13) do not hold) is included within the sampling volume, then $\langle [HO_2] \rangle / \langle [OH] \rangle$ will be further enhanced because $[HO_2]/[OH]$ in the background is so large ($\approx$35). It is for these reasons that this sampling effect leads to an increase in the measured ratio.

The effects of averaging strongly fluctuating concentrations over finite volumes will be reduced as the sizes of the sampling volumes are reduced, and removed entirely for point samples. Figures 8 and 9 are the same as Figures 5 and 6 but with the data now sampled strictly locally. This measurement is in much better agreement with the equilibrium predictions, showing how much the spatial averaging skewed the previous results. There are still significant differences, however, due to the inadequacy of the equilibrium approximations in large regions around the plume edges (as can be seen from

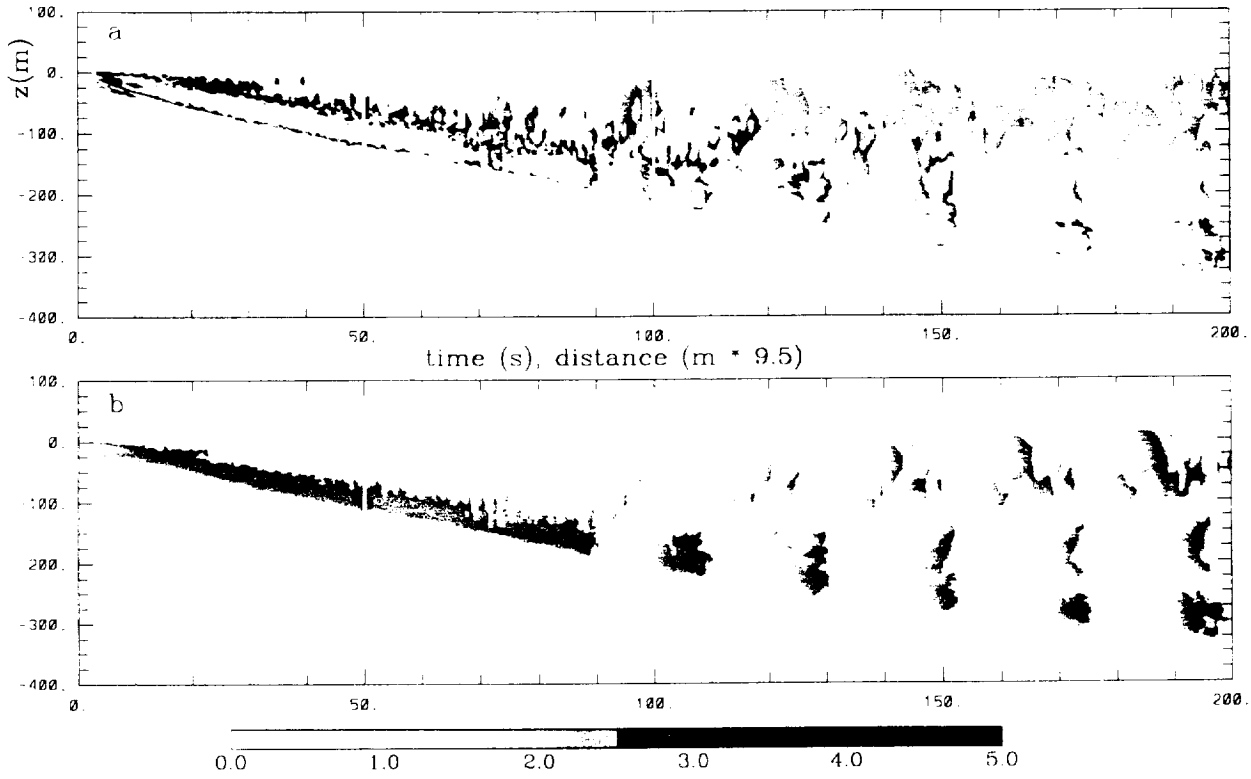

Figure 7. Concentration fields relative to background on a downstream space/time versus height slice for the simulated B757 wake: (a) OH (in ppt) and (b) HO_2 (in -5 ppt units).

the regions of enhanced OH in Figure 7). The mixing into the plume of background HO_2 can be an important source, via reaction (6), of OH in the plume (in addition to HONO photolysis as assumed in (12)). Here as well, where NO is lower, the exchange reactions between OH and HO_2 are not necessarily fast compared to the dynamics. Again this effect leads to larger $[HO_2]/[OH]$ ratio at a given NO level than predicted in equilibrium, because reaction (6) converting HO_2 to OH (pushing them to their equilibrium levels) is slowed relative to the dynamics mixing HO_2 into the region.

The nonequilibrium effect is largest for the young plume where the vortex-driven mixing is most vigorous, and becomes steadily less important in the aging plume as the turbulence levels fall. In contrast, the effect from sampling finite volumes involves fluctuations on different scales at different times during the evolution, and remains important out to later times. At early times, which tend to cover larger values of NO, the sharp edges of the engine exhaust and its instabilities contribute most to the effect, with fluctuations on scales of order 10 m or less. Subsequently, the engine exhausts get smoothed out somewhat by diffusion as they are more completely rolled into the vortex pair. The dominant downstream species fluctuations here are of intermediate scale arising from small axial pressure variations within the vortex cores (due to ambient turbulence). These fluctuations can be large for larger ambient turbulence levels (sometimes misrepresented as being due to vortex "breakdown" or "bursting") but are modest here. We see reduced sampling effects in Figure 5 for the wake age of 50 s. From about 60 s and later, the distribution is most strongly affected by the growth of the Crow instability of the vortex pair. The sampling effect in Figure 6 from these fluctuations (and presumably in the SUCCESS observations) is large because the sample length is approximately equal to the most favored wavelength for the Crow instability for this aircraft. At later times these induced fluctuations are slowly eroded down to a level consistent with the ambient turbulence as the wake slowly dilutes. By reducing the sampling size well below the Crow wavelength, the sampling effects could

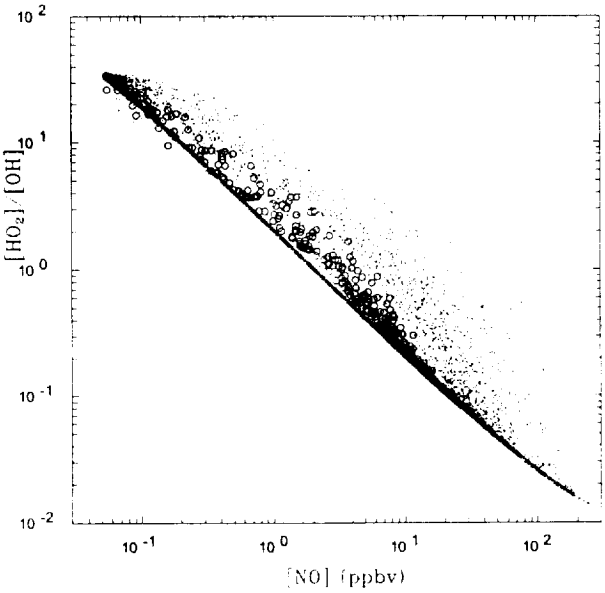

Figure 8. As in Figure 5, but using local point samples.

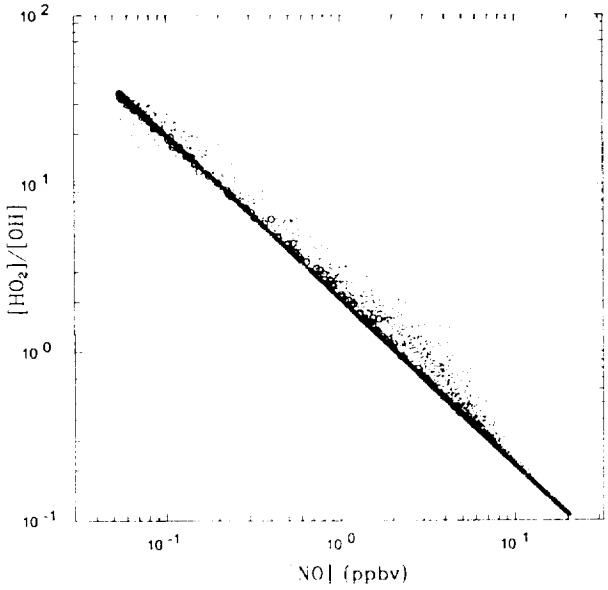

Figure 9. As in Figure 6, but using local point samples.

be significantly reduced for all but the earliest wake times.

It should be noted that we are almost certainly underestimating the effects of sampling over fluctuations in the very young wake versus those encountered in the SUCCESS measurements, for at least two reasons. First, we do not begin the simulation of the exhaust jets at their earliest and most intense phase, and so we underpredict the fluctuations from jet turbulence. Second, and probably more importantly, we have perfectly aligned our sampling lines along the initial wake axis, while the DC-8 sampling behind the B757 during SUCCESS would have had difficulty remaining centered within the small cross section of the young wake plume, especially given the large wake turbulence present there.

Finally, one apparent difference between Figure 2 of *Tan et al.* [1998] and our results deserves comment. As we have noted, when our measured $[HO_2]/[OH]$ ratio as a function of NO differs appreciably from the prediction of (11), it exceeds it (as is appropriate for the explanations of this effect given above). This is true for the bulk of the data points given by *Tan et al.* [1998] as well, but they also find a small fraction scattered below the expected values. These may just be stray data points (they quote a 1-σ precision for their data of 0.23 pptv for OH and 0.75 pptv for HO_2), indicate fluctuations not considered here in background levels of some species, or be due to the fact that the NO and HO_x probes on the DC-8 were not colocated but on the starboard and bottom of the fuselage, respectively.

4. Concluding Remarks

This LES of the near wake of a B757 provides a fine-grained chemical-dynamical representation of simplified NO_x -HO_x chemistry in the early wake. It demonstrates the feasibility of such simulations to investigate the potential impact of turbulent dynamic interactions with the wake chemical kinetics. By sampling the simulated data in a manner similar to that of in situ aircraft measurements, it is possible to interpret results obtained at the typical sampling rate of 1 Hz. In particular, comparison of these simulation results with actual in situ flight measurements of OH and HO_2 performed under cruise conditions in the upper troposphere during SUCCESS in May 1996 provides a likely explanation for the apparent large discrepancy between measurement and theoretical expectation found by *Tan et al.* [1998]. The discrepancy appears to be due to two effects of the wake dynamics on the measured chemistry: (1) the effect of averaging over species fluctuations on a scale smaller than can be resolved by the sampling rate, and (2) large turbulent mixing rates near the plume edges dramatically modifying the local equilibrium chemistry predictions. Both are accentuated by the dramatic difference in HO_2 concentration inside and outside of the wake

plume.

We have discussed the fluctuation problem principally from the point of view of a sampling size difficulty, but it is clear that any wake model has the same problem in averaging over large fluctuations within its representative volume elements. For a plume model with volume elements consistent with the data samples, we have confirmed the speculation of *Tan et al.* [1998, p. 1723] that "turbulent fluctuations in the plume may significantly reduce reaction rates between species which are anti-correlated in distribution, such as between NO and HO_2." Even in our unsteady, 3-D, high-resolution model, there are probably some volume elements around the edges of the wake where fluctuations with significant anticorrelation between NO and HO_2 occur. To correct this, it would be necessary to use even higher resolution, or to introduce the major effect of the fluctuations into a subgrid model of the chemical kinetics. Since the reaction in (6) depends on the average of the product of NO and HO_2 rather than the product of their averages, the effective reaction rate will be increased (reduced) by fluctuations when they are correlated (anticorrelated). Progress has been made toward generating models which include the influence of the unresolved covariance of the reactants within a model [e.g., *Sykes et al.*, 1994], but a robust model for general conditions remains a challenging problem. In our high-resolution model we believe neglecting such effects only influences the sharpness of the wake edges, but in 2-D models where all of the downstream 3-D structure is averaged out in the model wake representation [e.g., *Anderson et al.*, 1996], the uncertainty expected should be similar to that found in the in situ measurements.

In contrast to the strong influence the fluctuations have on HO_x chemistry, the influence on the NO_x - O_3 chemistry is relatively benign. For the conditions of this simulation, dilution of the wake tends to be faster than the rate at which NO within the wake destroys the O_3, so a relatively small O_3 deficit is generated within the wake. It is not sufficiently strong to yield a strong anticorrelation between NO and O_3 within the fluctuations. Thus the basic effect of the turbulence is straightforward dilution of the wake which can be captured by relatively simple Gaussian plume models of the wake [e.g., *Karol et al.*, 1997]. This would not be true if the emission of the NO_x was an order of magnitude larger or the dilution rate an order of magnitude smaller.

The simulation presented was performed on a desktop workstation (a 566 MHz Alpha CPU with 512 Mb of ram) using just over 4 days of CPU time, so it is quite feasible to do other simulations dealing with more complicated chemical pathways of possible interest, and/or early jet or late plume chemistry. The transition regime between plume models and 3-D global models presents a particular challenge given the potential importance of turbulent mixing and large species fluctuations occurring on scales below typical grid lengths, of order 100 km, which can be employed. We would not recommend attempting such a simulation at resolutions capable of resolving individual plumes while maintaining around 100 possible chemical interactions, but it should be possible to include the chemical kinetics associated with 10-20 critical species to estimate the uncertainty associated with neglecting all of the subgrid fluctuations.

Acknowledgment. This work was supported by NASA grant NAG-1-2096 as part of NASA's Atmospheric Effects of Aviation Project, with Bill Grose and Bruce Anderson as technical monitors.

References

Anderson, M. R., R. C. Miake-Lye, R. C. Brown, and C. E. Kolb, Calculation of exhaust plume structure and emissions of the ER2 aircraft in the stratosphere, *J. Geophys. Res.*, *101*, 4025–4032, 1996.

Brown, S. B., R. Talukdar, and A. R. Ravishankar, Rate constants for the OH + NO_2 + M $\longrightarrow$ HNO_3 + M under atmospheric conditions. *Chem. Phys. Lett.*, *299*, 277–284, 1999.

Campos, T., et al., Measurement of NO and NO_y emission indices during SUCCESS, *Geophys. Res. Lett.*, *25*, 1713–1716, 1998.

Chlond, A., Large-eddy simulations of contrails, *J. Atmos. Sci.*, *55*, 796–819, 1998.

Crow, S. C., Stability theory for a pair of trailing vortices, *AIAA J.*, *8*, 2172–2179, 1970.

DeMore, W. B., S. P. Sander, C. J. Howard, A. R. Ravishankara, D. M. Golden, C. E. Kolb, R. F. Hampson, M. J. Kurylo, and M. J. Molina (Eds.), Chemical kinetics and photochemical data for use in stratospheric modeling, *JPL Pub. 97-4*, 1997.

Farnell, L., Solution of Poisson equations on a nonuniform grid, *J. Comput. Phys.*, *35*, 408–425, 1980.

Friedl, R. R. E., Atmospheric effects of subsonic aircraft: Interim assement report of the advanced subsonic technology program, *NASA Ref. Pub. 1400*, 1997.

Gerz, T., and T. Ehret, Wake dynamics and exhaust distribution behind cruising aircraft, *AGARD Symp. Proc., CP-584*, 35.1–35.12, 1996.

Gerz, T., T. Dürbeck, and P. Konopka, Transport and effective diffusion of aircraft emissions, *J. Geophys. Res.*, *103*, 25,905–25,913, 1998.

Gierens, K. M., Numerical simulations of persistent contrails, *J. Atmos. Sci.*, *53*, 3333–3348, 1996.

Gierens, K. M., and E. Jensen, A numerical study of the contrail–to–cirrus transition, *Geophys. Res. Lett.*, *25*, 4341–4344, 1999.

Jaegle, L., D. Jacob, W. Brune, D. Tan, I. C. Faloona, A. Weinheimer, B. Ridley, T. Campos, and G. Sachse, Sources of HO_2 and production of ozone in the upper troposphere over the United States, *Geophys. Res. Lett.*, *25*, 1709–1712, 1998.

Kärcher, B., R. Busen, A. Petzold, F. Schröder, U. Schumann, and E. Jensen, Physicochemistry of aircraft–generated liquid aerosols, soot, and ice particles, 2, Comparison with observations and sensitivity studies, *J. Geophys. Res.*, *103*, 17,129–17,147, 1998.

Karol, I. L., Y. E. Ozolin, and E. V. Rozanov, Box and Gaussian plume models of the exhaust composition evolution of the subsonic transport aircraft in and out of the flight corridor, *Ann. Geophys.*, *15*, 88–96, 1997.

Lewellen, D. C., and W. S. Lewellen, Large-eddy simulations of the vortex-pair breakup in aircraft wakes, *AIAA J.*, *34*, 2337–2345, 1996.

Lewellen, D. C., and W. S. Lewellen, The effects of aircraft wake dynamics on contrail development, *J. Atmos. Sci.*, *58*, 390–406, 2001.

Lewellen, D. C., W. S. Lewellen, L. R. Poole, R. J. DeCoursey, G. M. Hansen, and C. A. Hostetler, Large-eddy simulations and lidar measurements of vortex-pair breakup in aircraft wakes, *AIAA J.*, *36*, 1439–1445, 1998.

Lewellen, D. C., W. S. Lewellen, and J. Xia, The influence of a local swirl ratio on tornado intensification near the surface, *J. Atmos. Sci.*, *57*, 527–544, 2000.

Menon, S., and J. Wu, Effects of micro- and macroscale turbulent mixing on the chemical processes in engine exhaust plumes. *J. Appl. Meteorol.*, *37*, 639–654, 1998.

Miake-Lye, R. C., M. Martinez-Sanchez, R. C. Brown, and C. E. Kolb, Plume and wake dynamics, mixing and chemistry behind a high speed civil transport aircraft, *J. Aircr.*, *30*, 467–479, 1993.

Penner, J. E., D. H. Lister, D. J. Griggs, D. J. Dokken, and M. McFarland (Eds.), *Aviation and the Global Atmosphere*, Cambridge Univ. Press, New York, 1999.

Quackenbush, T. R., M. E. Teske, and A. J. Bilanin, Dynamics of exhaust plume entrainment in aircraft vortex wakes, *AIAA Pap. 96-0747*, Am. Inst. of Aeronaut. and Astronaut., New York, 1996.

Schumann, U., Large-eddy simulation of turbulent diffusion of chemical reactions in the convective boundary layer, *Atmos. Environ.*, *23*, 1713–1727, 1989.

Schumann, U., The impact of nitrogen oxides emissions from aircraft upon the atmosphere at flight altitudes: Results from the AERONOX project, *Atmos. Environ.*, *31*, 1723–1734, 1997.

Schumann, U., Research on the effect of aircraft and spacecraft upon the atmosphere, *Atmos. Environ.*, *31*, 3065–3066, 1998.

Singh, H. B., A. M. Thompson, and H. Schlager, SONEX airborne mission and coordinated POLINAT-2 activity: Overview and accomplishments, *Geophys. Res. Lett.*, *26*, 3053–3056, 1999.

Spalart, P. R., Airplane trailing vortices, *Annu. Rev. Fluid Mech.*, *30*, 107–138, 1998.

Spalart, P. R., and A. A. Wray, Initiation of the Crow instability by atmospheric turbulence, *AGARD Symp. Proc.*, *CP-584*, 18.1–18.8, 1996.

Sussmann, R., and K. M. Gierens, Lidar and numerical studies on the different evolution of vortex pair and secondary wake in young contrails, *J. Geophys. Res.*, *104*, 2131–2142, 1999.

Sussmann, R., and K. M. Gierens, Differences in early contrail evolution of two-engine versus four-engine aircraft: Lidar measurements and numerical simulations, *J. Geophys. Res.*, *106*, 4899–4911, 2001.

Sykes, R. I., and D. S. Henn, Large-eddy simulation of turbulent sheared convection, *J. Atmos. Sci.*, *46*, 1106–1118, 1989.

Sykes, R. I., D. S. Henn, S. F. Parker, and W. S. Lewellen, Large-eddy simulation of a turbulent reacting plume, *Atmos. Environ.*, *26A*, 2565–2574, 1992.

Sykes, R. I., S. F. Parker, D. S. Henn, and W. S. Lewellen, Turbulent mixing with chemical reaction in the planetary boundary layer, *J. Appl. Meteorol.*, *33*, 825–834, 1994.

Tan, D., I. Faloona, W. Brune, A. Weinheimer, T. Campos, B. Riley, S. Vay, J. Collins, Jr., and G. Sachse, In situ measurements of HO_x in aircraft exhaust plumes and contrails during SUCCESS, *Geophys. Res. Lett.*, *25*, 1721–1724, 1998.

Toon, O. B., and R. C. Miake-Lye, Subsonic Aircraft: Contrail and Cloud Effects Special Study (SUCCESS), *Geophys. Res. Lett.*, *25*, 1109–1112, 1998.

Vay, S., et al., DC-8-based observations of aircraft CO, CH_4, N_2O, and $H_2O_{(g)}$ emission indices during SUCCESS, *Geophys. Res. Lett.*, *25*, 1717–1720, 1998.

D. C. Lewellen and W. S. Lewellen, Department of Mechanical and Aerospace Engineering, West Virginia University, P.O. Box 6106, Morgantown, WV 26506-6106, USA. (dlewelle@wvu.edu; wlewelle@wvu.edu)

Received February 21, 2001; revised June 28, 2001; accepted July 4, 2001.